ACS Macro Letters

pubs.acs.org/macroletters Letter

Multiphase Coacervates Driven by Electrostatic Correlations

Xu Chen, Er-Qiang Chen,* An-Chang Shi,* and Shuang Yang*

Cite This: *ACS Macro Lett.* 2021, 10, 1041−1047 Read Online

ACCESS | Metrics & More | Article Recommendations | Supporting Information

ABSTRACT: The liquid−liquid phase separation of a polyelectrolyte solution containing one type of negatively and two types of positively charged polymers with different charge densities is studied theoretically by random phase approximation (RPA). It is predicted that multicoacervate phases could coexist, driven purely by electrostatic correlations. The asymmetry of the linear charge density could induce an effective immiscibility between two positively charged polyelectrolytes, leading to the multiphase separation. Adding salt will induce the disappearance of the dilute phase, forming two coexisting complex phases, instead of fusion between coacervates. Raising temperature could either induce a two coexisting complex phase, or a dilute phase coexisting with a coacervate phase, depending on the bulk concentration. Our predictions are in good agreement with experiments and provide insights in the further designing of the multiphase coacervation system.

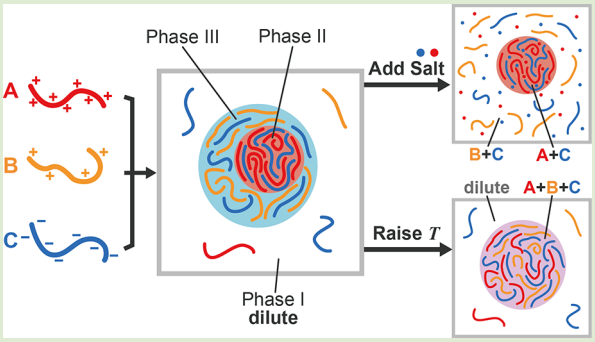

Liquid−liquid phase separation is believed to play a key role in the formation of various membraneless organelles, which are essential in certain cellular processes.[1,2] One important route of liquid−liquid phase separation is via the associative phase separation of oppositely charged polyelectrolytes, known as complex coacervation.[3−5] Polymer-rich coacervate phases may coexistence with a supernatant phase, resulting from the electrostatic correlation induced attraction between the charged species.[6−10] The basic modeling system for complex coacervation consists of two oppositely charged polyelectrolytes, and its phase behavior is well studied. First, the Voorn−Overbeek (VO) theory,[11] or VO-based theory,[12] was a primary way to capture the Debye−Hückel attraction of a simple electrolyte, while it fails to correctly describe free energy for complex coacervates, as it ignores many factors, especially the chain connectivity. The random phase approximation (RPA) considering the chain connectivity and intramolecular correlation[13−17] was then developed. However, RPA is inadequate in describing the dilute phase due to the ideal chain assumption. Many advanced theories, including the liquid state theory,[18,19] transfer matrix theory,[20] scaling law,[21] field theoretic simulations,[22] and renormalized Gaussian fluctuation,[23] have been developed to obtain the qualitative or quantitative understanding of the electrostatic correlation effects.[24]

In reality, the intracellular phase separation always involves multicomponent systems. The emergence of coexisted multiphase droplets was confirmed by a number of experiments.[25−30] These multicoacervate phases have the potential to enrich different kinds of solutes,[28] leading to distinct circumstances for biochemical reactions,[31] and is vital in membraneless organelles' complex functions such as RNA processing.[25] Nevertheless, the origin of immiscibility among the different dense phases formed by charged macromolecules remains controversial.[26] A large number of existing studies[32−35] attribute the separation of different coacervate phases to the χ parameters between them, usually based on the framework of the Flory−Huggins model. Indeed, the simulations with varied short-range interactions of each species exhibit the core−shell multiphase structures.[27] However, some recent works revealed that the formation of multiphase droplets could be driven by long-range electrostatic interaction.[29,36] When coexisting coacervate phases form a core−shell structure, the strong polyelectrolytes with higher linear charge density are thought to be located in the inner part, while weakly charged polymers comprise the shell.[36] However, how to control the multiphase separation driven by an electrostatic interaction and what is the underlying mechanism remain unclear. In this Letter, we report a systematic theoretical investigation for the complex coacervation of three-component polyelectrolyte solutions, demonstrate that multiphase separation could be driven solely by electrostatic fluctuation, and show the effect of salt concentration and temperature in this process.

Received: April 27, 2021
Accepted: July 23, 2021
Published: July 27, 2021

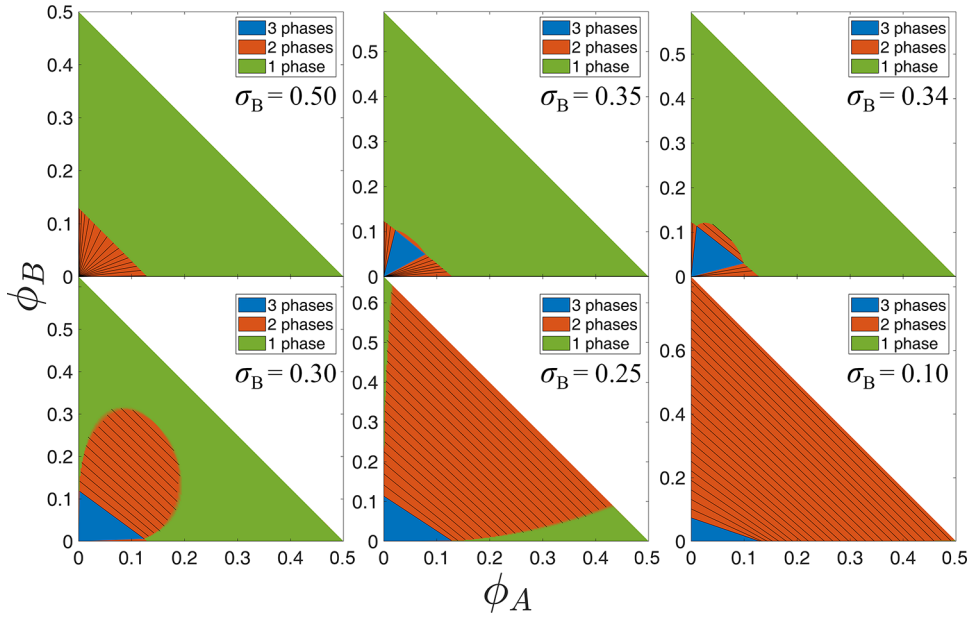

Figure 1. Phase diagram of the salt-free solution of polycations A and B and polyanion C. $N_A = N_B = N_C = 100$, $\sigma_A = \sigma_C = 0.5$, and $\sigma_B = 0.50$, 0.35, 0.34, 0.30, 0.25, and 0.10. $\phi_C = (\phi_A\sigma_A + \phi_B\sigma_B)/\sigma_C$. All the Flory–Huggins parameters χ are set to 0. Blue, red, and green denote the three-phase, two-phase, and single-phase regions, respectively. Black lines of the two-phase region are tie-lines of phase separation.

In order to account for the electrostatic correlation of polyelectrolytes, we adopt RPA theory in which polyelectrolytes assume Gaussian chain conformation. As the correlation function is in good agreement with a Gaussian chain for a dense solution of weakly charged polyelectrolytes,[22] RPA can quantitatively capture the properties of coacervate phase.[37] For the dilute phase, however, RPA ignores some important high-order fluctuation corrections and the coupling between electrostatic fluctuations and chain conformation, so more accurate theories, such as field theoretic simulation[22] or renormalized Gaussian fluctuation,[38] are then needed. We consider aqueous solutions of two types of weakly charged polycations (denoted as A and B chains) and one polyanion C. These polyelectrolytes consists of N_A, N_B, or N_C monomers, respectively. All polyelectrolytes have the same Kuhn length b (set as length unit), which is equal to 0.85 nm, consistent with a hydrated monomeric unit length.[39] The solvent (denoted as S) is assumed to have the same volume as a monomer. The charges are smeared so that each monomer of polyelectrolyte species I has a uniform charge density σ_I (I = A, B, C). The negative charges of C are assumed to be compensated by the positive charges of A and B to guarantee the overall charge neutrality condition. The counterions or salt ions are not distinguished and monovalent. Each small ion (denoted as s) is point-like and carries a charge e. The density of each molecule i is ρ_i and its volume fraction concentration is $\phi_i = \rho_i b^3$. In terms of RPA,[14,15] the free energy density f of a homogeneous phase can be written as

$$f \equiv \frac{F}{Vk_BT} = f_{\text{F-H}} + f_{\text{RPA}} \tag{1}$$

where F is the free energy, V is the system volume, k_B is the Boltzmann's constant, and T is the absolute temperature and will be set to 300 K. The first term in eq 1 represents the mean-field contribution and assumes the Flory–Huggins form:

$$f_{\text{F-H}} = \sum_i \frac{\phi_i}{N_i} \ln \phi_i + \frac{1}{2}\sum_{ij} \phi_i\phi_j\chi_{ij} \tag{2}$$

where the summations run over all species (A, B, C, S, s). The second term in eq 1 is the electrostatic correlation energy computed with RPA and it is given by

$$f_{\text{RPA}} = \frac{b^3}{2}\int \frac{d\mathbf{q}}{(2\pi)^3}\left[\ln\left(1 + \sum_i \rho_i g_i(\mathbf{q})u(\mathbf{q})\sigma_i^2\right) - \sum_s \rho_s u(\mathbf{q})\sigma_s^2\right] \tag{3}$$

Here $g(\mathbf{q})$ denotes the intramolecular monomer–monomer correlation function. For a Gaussian chain, it has the form $g_i(\mathbf{q}) = 2\{\exp(-x) - 1 + x\}/x^2$, $x = q^2b^2N/6$. For small ions, $g(\mathbf{q}) = 1$. $u(\mathbf{q}) = 4\pi l_B/q^2$ represents the Coulomb interaction between two elementary charges, where the Bjerrum length $l_B = e^2/(\varepsilon_0\varepsilon_r k_B T)$. ε_0 is the vacuum permittivity and ε_r is the relative dielectric constant ($\varepsilon_r \approx 78$ for water).

For a given free energy density (eq 1), the convex hull method (see details in ref 40) is used to construct phase diagrams of multicomponent mixtures. First, we investigate the three-component (A, B, C) polyelectrolyte solution without small ions. For simplicity, the chain length of polyelectrolytes is set as $N_A = N_B = N_C = 100$, and the charge density of A and C is $\sigma_A = \sigma_C = 0.5$; $l_B = 0.7$ nm. All the Flory–Huggins parameters χ_{ij} are set to 0 to highlight the electrostatic interaction effect. These parameters are fixed in this study unless specified otherwise. The phase diagrams are calculated with varying σ_B. Figure 1 displays typical phase diagrams in the (ϕ_A, ϕ_B) parameter space at different σ_B. When $\sigma_B = \sigma_A = 0.5$, there is no three-phase coexistence region, as expected. In the two-phase (red) region, the solution may separate into a dilute phase and a condensed phase composed of A, B, and C (the black lines represent tie lines, which label the compositions of two coexisting phases), consistent with the normal bicomponent coacervation since B is identical to A. Significantly, the three-phase (blue) region appears when σ_B is lowered to 0.35. In this region, the solution phase separates into a dilute phase,

https://doi.org/10.1021/acsmacrolett.1c00282
ACS Macro Lett. 2021, 10, 1041−1047

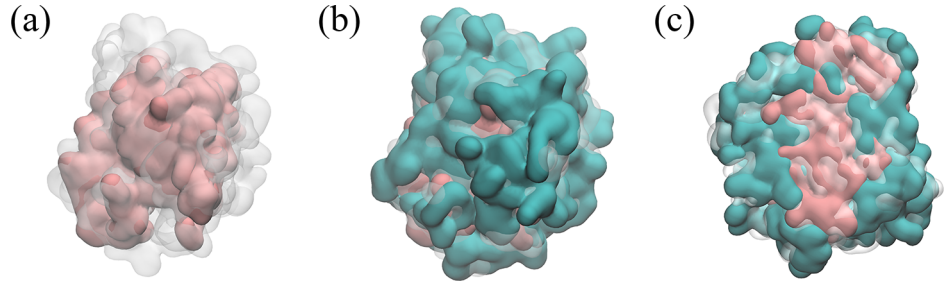

Figure 2. Molecular dynamics simulations for the system where $N_A = N_B = N_C = 40$, and each monomer of A, B, and C has a charge of +0.5, +0.2, and −0.5. Red, cyan, and transparent surface denote A, B, and C, respectively. Diagrams show the surface of (a) A and C and (b) A, B, and C. The snapshot of the cross-section at the midpoint is displayed in (c).

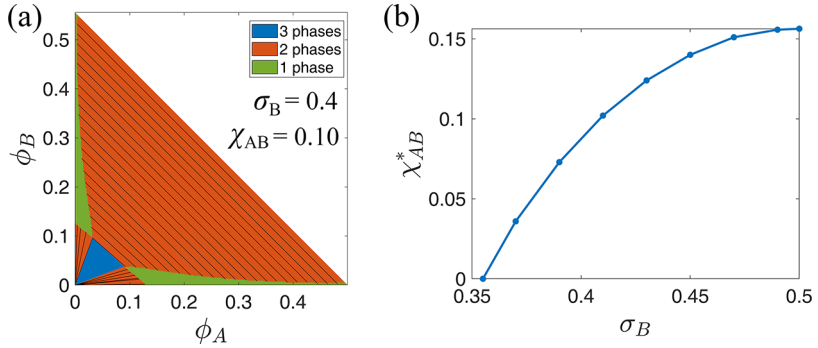

Figure 3. (a) Phase diagram of polycations A and B and polyanion C solution. $N_A = N_B = N_C = 100$, $\sigma_A = \sigma_C = 0.5$, $\sigma_B = 0.4$, and $\chi_{AB} = 0.10$; (b) The critical value χ_{AB} to induce multiphase separation for different σ_B. When $\sigma_B < 0.355$, pure electrostatic interaction is enough to induce the multiphase separation.

a AC-rich coacervate phase and a BC-rich coacervate phase (denoted as phases I, II, and III, respectively), shown as the three vertexes of the blue triangle. With further decreasing σ_B, the separated AC−BC two-phase (red) region becomes larger, while the three-phase region expands first and then shrinks because low enough σ_B will produce a small concentration of *B* in phase II. In the three-phase region, A and B chains become almost immiscible, and they complex with C polymers separately. The electrostatic interaction driven triple-phase separation is further verified using molecular dynamics (MD) simulations. We consider a system with $N_A = N_B = N_C = 40$, and each monomer of A, B, and C has a charge of +0.5, +0.2, and −0.5, respectively. The MD simulation results are shown in Figure 2. Charged polymers aggregate together and form complexes. Within the aggregate, A chains (red) are concentrated in the core part and B chains (cyan) are distributed in the outer region, showing the macrophase separation between the core consisting of the AC phase and the shell consisting of the BC phase. Both the RPA method and the MD simulation confirm that the difference in linear charge density of polymers does induce multiphase separation without any short-range interaction of $\chi = 0$.

To reveal the mechanism behind the phase separation within the coacervate, we analyze the effective immiscibility due to the asymmetric linear charge densities. In the absence of an electrostatic interaction, the second-order variation of free energy density takes the following form:

$$\delta^2 f_{\text{F-H}} = \sum_i \frac{1}{N_i \phi_i} \delta\phi_i^2 + \frac{1}{2}\sum_{ij} \chi_{ij} \delta\phi_i \delta\phi_j \tag{4}$$

Adding the contribution from the electrostatic correlation, the additional second-order variation due to eletrostatics is given by

$$\delta^2 f_{\text{RPA}} = -\sum_{ij} \frac{1}{2} \int \mathrm{d}\mathbf{q}[a(\mathbf{q}) g_i(\mathbf{q}) g_j(\mathbf{q}) \sigma_i^2 \sigma_j^2] \delta\phi_i \delta\phi_j \tag{5}$$

where $a(\mathbf{q})$ runs over all charged species *m* and is independent of specific *i*, *j*,

$$a(\mathbf{q}) \equiv \frac{u(\mathbf{q})^2 b^3}{\left(b^3 + \sum_m \phi_m g_m(\mathbf{q}) u(\mathbf{q}) \sigma_m^2\right)^2} \tag{6}$$

Adding these two contributions results in the effective interaction parameters $\chi_{\text{eff},ij}$,

$$\chi_{\text{eff},ij} \equiv \chi_{ij} - \int \mathrm{d}\mathbf{q}(a(\mathbf{q}) g_i(\mathbf{q}) g_j(\mathbf{q}) \sigma_i^2 \sigma_j^2) \tag{7}$$

Using the incompressibility constrain $\sum_i \delta\phi_i = 0$, we further modify the matrix $\chi_{\text{eff},ij}$ to $\chi'_{\text{eff},ij}$ so that the diagonal elements $\chi'_{\text{eff},ii} = 0$; meanwhile, $\delta^2 f$ keeps constant. If all chains have an identical length, $\chi'_{\text{eff},ij}$ takes the form

$$\chi'_{\text{eff},ij} = \chi_{ij} + \frac{1}{2}(\sigma_i^2 - \sigma_j^2)^2 \int \mathrm{d}\mathbf{q} a(\mathbf{q}) g^2(\mathbf{q}) \tag{8}$$

During the complexation process of the multicomponent solution, polyanion C has stronger attraction toward A and weaker attraction toward B. This difference in attractions induces repulsion between the A and B chains. In terms of eq 8, a large enough difference in charge fraction between two species could lead to a positive χ_{eff}, resulting in strong immiscibility that drives the multiphase separation. Therefore, the roles of electrostatic correlation are 2-fold, producing

https://doi.org/10.1021/acsmacrolett.1c00282
ACS Macro Lett. 2021, 10, 1041−1047

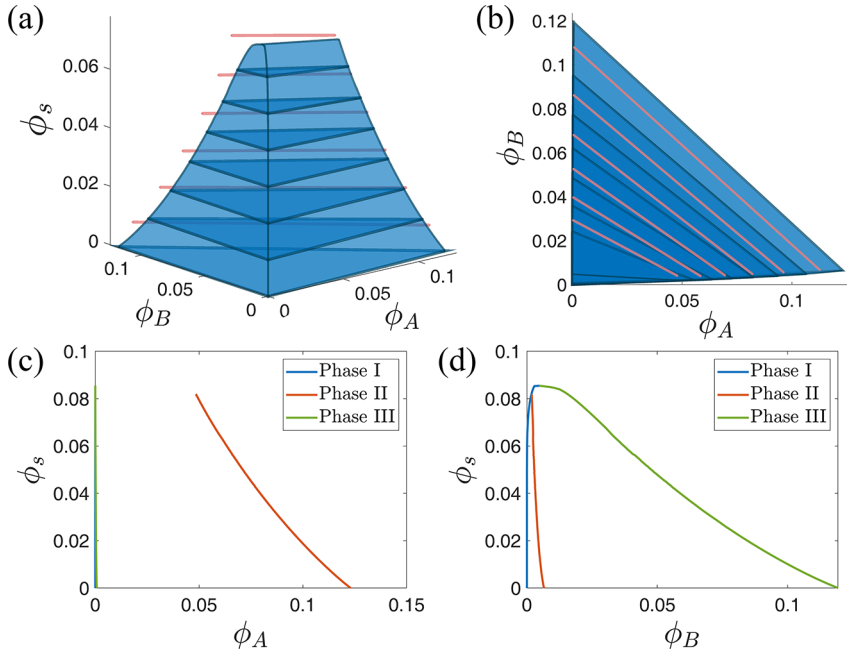

Figure 4. (a) Phase diagram of a solution of polycation A and B and polyanion C when salt is added. $\sigma_B = 0.3$. The blue region denotes the three-phase separation. The deep blue surface denotes the tie lines of the three-phase separation, and red lines are some typical tie lines of the two-phase separation. (b) Top view of phase diagram (a). (c) ϕ_A and (d) ϕ_B in each phase. Blue, red, and green lines denote phases I, II, and III, respectively.

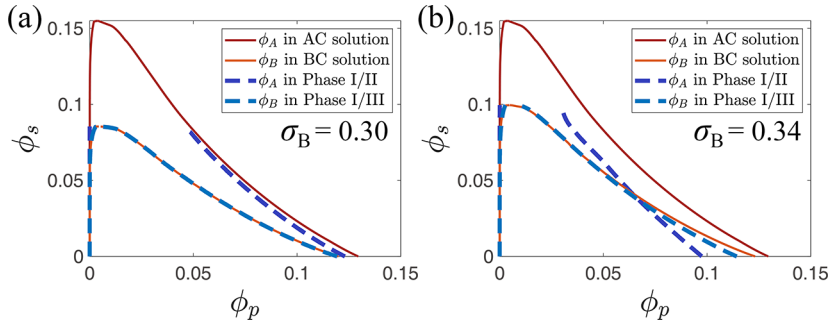

Figure 5. Comparison of the A and B concentrations in different coacervation processes. Solid lines are from the coacervation of individual AC or BC bicomponent solution, and dash lines are from the coacervation of the ABC mixture solution. $N_A = N_B = N_C = 100$, $\sigma_A = \sigma_C = 0.5$, and (a) $\sigma_B = 0.3$, (b) $\sigma_B = 0.34$.

attraction between charged polymers by making solvents poorer and bringing additional immiscibility for chains with asymmetric charge densities. The phase separation between A and B chains originates from the latter effect.

Based on a previous analysis, we expect that the difference of σ may bring similar effect as χ between different species. Consequently, the formation of multiphase separation could be induced by a combination of varying σ and χ. As an example, we consider a system having the same parameters as Figure 1 but with $\sigma_B = 0.4$, in which the difference of σ_A and σ_B is inadequate to induce a triple-phase separation. However, if one increases χ_{AB} from 0 to $\chi_{AB} = 0.10$, the three-phase region will appear as shown in Figure 3a. For the same N and σ_A and σ_C, we calculated the critical value χ^*_{AB} required to form the three-phase region as a function of σ_B in Figure 3b. When $\sigma_B > 0.355$, triple-phase separation will happen only for a positive χ_{AB} larger than χ^*_{AB}. It is expected that the observed multiphases in the experiments may be driven by either these two factors or their combination.

The electrostatic interaction can be screened by the addition of salts. For a common bicomponent polyelectrolyte blend, the coacervate phase may swell and dissolve at critical salt concentration (CSC).[41] We investigate the salt effect on the three-phase region of the triple component system. The detailed calculation, including salt ions, is given in the Supporting Information. The salt includes an equivalent cation and anion, and the concentration is $\phi_s = \phi_s^+ = \phi_s^-$. Figure 4 shows the three-dimensional phase diagram for $\sigma_B = 0.3$. With increasing salt concentration, the three-phase region gradually shrinks and finally disappears, similar to the case of the bicomponent coacervation. The concentration of salt ions partitioned in coacervate is first slightly higher and then lower than that of dilute phase (details in the Supporting Information). Also, the two coexisted phases II and III exhibit strong separation between the A and B chains, since phase II hardly contains B chains and vice versa (Figure 4c,d).

Intuitively, one may argue that the three-phase separation of the ABC mixture could be regarded as the blending of two separate phase separations (AC and BC mixtures).[29] We further give the compositions of each coacervate phase by comparing a three-phase separation process with an individual A+C or B+C complex coacervate, which is shown in Figure 5.

https://doi.org/10.1021/acsmacrolett.1c00282
ACS Macro Lett. 2021, 10, 1041−1047

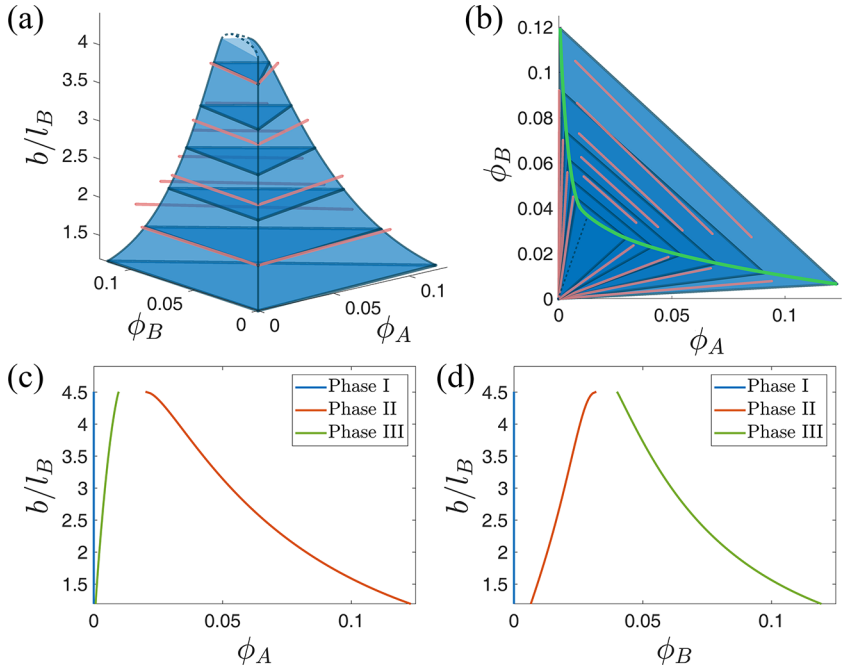

Figure 6. (a) Phase diagram of the solution of polycation A, B, and polyanion C when raising the temperature. $\sigma_B = 0.3$. The blue region denotes a three-phase separation. The deep blue surface denotes the tie lines of a three-phase separation, and red lines are some typical tie lines of a two-phase separation. The dot lines are drawn to guide the eye. (b) Top view of phase diagram (a). When the three-phase separation turns into two-phase, the region below the green line denotes a dilute ABC separation, and above it denotes AC−BC separation. (c) ϕ_A and (d) ϕ_B in each phase. Blue, red, and green lines denote phases I, II, and III, respectively.

The dash lines give the concentration of A (or B) in phases I and II (or phase III) of the three-phase separation, and the solid lines are from the individual A+C or B+C complex coacervation. Apparently, for a largely distinct charge density of $\sigma_B = 0.3$, the three-phase separation is almost equal to two individual coacervations. This situation is in accord with the early study.[29] As phase III contains little A chains, the two curves of the B concentration perfectly overlap, while curves of A show a slight shifting because of a small amount of B chains contained in phase II. Once $\sigma_B = 0.34$, close to the critical value $\sigma_B^* = 0.355$ of the multiphase separation, the separation tendency of A and B chains becomes weak, leading to a higher concentration of B chains in phase II. In this case, the assumption of two individual phase separations of the coexisting three phases breaks down. On the other hand, the coexisting of two coacervates is related to the immiscibility between them. It was proposed that the associated large difference in critical salt concentrations of two coacervates (c_1^*, c_2^*) provides immiscibility and causes their demixing in solution through an effective χ parameter by $\chi_{12} \sim (1/\sqrt{c_1^*} - 1/\sqrt{c_2^*})^2$.[29] For two coacervates with an identical CSC, multiphase droplets should not be observed. However, our calculation shows that three-phase coexisting may still occur in some cases; even the two coexisted and well-separated coacervate phases have the same CSC (see Supporting Information). Therefore, the difference in CSC may not be a suitable criterion for the formation of multiphase droplets. An accurate estimation for immiscibility requires an analysis accounting for molecular details.

Figure 4 also indicates the salt effect on the phase coexistence. When more salt is added, the total composition is out of the blue three-phase region and the solution becomes two separated phases, then the tie lines (red) of a two-phase region shows that usually dilute phase I vanishes and coacervate phases II and III become two coexisted AC and BC solutions. On the other hand, if the bulk concentration of each species is relatively low, which is the general situation in experiments, phase III of the three phases will change into a BC dilute solution coexisting with phase II. This phenomenon is evidenced by Liang's work.[42] For a droplet including two coacervates, they found that the outer coacervate phase is first dissolved with increasing NaCl concentration, leaving the core coacervate unchanged. Besides, under the addition of salts, this preferential phase I−III fusion instead of the fusion between two coacervates still keeps, even though phases II and III show a weak separation tendency. For $\sigma_B = 0.34$, very close to the critical σ_B^*, the fusion of phase I−III is still prior to the fusion of phase II−III (see Supporting Information). Although the attractive electrostatic force between A/B and C chains should be weakened by the addition of salt, unexpectedly, A chains are always excluded from the BC-rich phase. The electrostatic fluctuation-driven immiscibility between A and B chains seems to be relatively unaffected by salt.

Ignoring the changing of χ and ε_r,[43] raising the temperature usually shows a similar effect to the addition of salt, both of which could weaken electrostatic attraction.[44] But in a multiphase separation system, the temperature has a distinct influence. Figure 6 displays the phase diagram calculated for a system with $\sigma_B = 0.3$. With increasing temperature (by decreasing l_B), the three-phase region (blue) shrinks and then vanishes, similar to adding salt. However, the dissolution way of multiphase depends on initial bulk concentrations. When initial concentrations lie above the region of the green line in Figure 6b, phase I disappears. At the same time, two coacervates are transformed into coexisting AC and BC solution phases with tie lines (red) of two-phase regions, like the addition of salt. However, when polymer concentrations

https://doi.org/10.1021/acsmacrolett.1c00282
ACS Macro Lett. 2021, 10, 1041−1047

are below the green line, raising the temperature leads to the fused coacervates of phases II and III coexisting with a dilute phase. A larger σ_B produces an expanded AC−BC fusion region (see Supporting Information). Both salt and temperature can weaken the electrostatic-driven immiscibility χ_{eff} by decreasing $a(\mathbf{q})$. Raising the temperature decreases the whole $u(\mathbf{q})$, while adding salts adds an extra $\phi g u \sigma^2$ term in the numerator of eq 6. This subtle difference between salt and temperature might finally result in a distinct phase behavior.

In summary, we investigated the liquid−liquid phase separation of multicomponent polyelectrolytes in solution and focused on the formation and dissolution of multiphase coacervates. We confirmed that the differences in the linear charge density of different polymers alone could drive the phase separation into the coexisting two coacervates due to induced different electrostatic correlations. Besides, adding salts only causes the dissolution of one coacervate phase with weaker charged polymers into the dilute phase, while raising the temperature may give rise to the fusion of two coacervate phases coexisting with dilute phase at low bulk concentration. The other factors that affect electrostatic interaction, such as charge sequence,[45,46] may also be able to induce the formation of a multiphase coacervation, which will be discussed in our future work. Another important issue is the deviation from the non-Gaussian chain statistics of polyelectrolytes in the coacervate phase, which may become important if the oppositely charged chains are asymmetrical enough in charge density,[21] bond length,[47] and stiffness.[48] Considering the charge density difference, a crude estimation based on scaling theory[21] shows that when $\sigma_C/\sigma_B \leq 2^{4/3} = 2.52$, the deviation from Gaussian statistic is unimportant (see Supporting Information for details). In our system, the deviation is not significant, and we ignore this effect. Our results provide some insights in understanding the mechanism of multiphase structure in membraneless organelles and can help to design an artificial multiphase-separated structure.

■ ASSOCIATED CONTENT

Supporting Information

The Supporting Information is available free of charge at https://pubs.acs.org/doi/10.1021/acsmacrolett.1c00282.

The details of calculation and simulation; the validity of ideal Gaussian chain statistics; the radial density profiles of monomers of coacervate in the simulation; phase diagrams when σ_B = 0.34; phase diagram of the coexisting three phases for ϕ_p in log scale; salt partition in each phase; the discussion about the validity of χ_{eff} (PDF)

■ AUTHOR INFORMATION

Corresponding Authors

Er-Qiang Chen − *Beijing National Laboratory for Molecular Sciences, Key Laboratory of Polymer Chemistry and Physics of Ministry of Education, Center for Soft Mater Science and Engineering, College of Chemistry and Molecular Engineering, Peking University, Beijing 100871, China;* orcid.org/0000-0002-0408-5326; Email: eqchen@pku.edu.cn

An-Chang Shi − *Department of Physics and Astronomy, McMaster University, Hamilton, Ontario L8S 4M1, Canada;* orcid.org/0000-0003-1379-7162; Email: shi@mcmaster.ca

Shuang Yang − *Beijing National Laboratory for Molecular Sciences, Key Laboratory of Polymer Chemistry and Physics of Ministry of Education, Center for Soft Mater Science and Engineering, College of Chemistry and Molecular Engineering, Peking University, Beijing 100871, China;* orcid.org/0000-0002-5573-5632; Email: shuangyang@pku.edu.cn

Author

Xu Chen − *Beijing National Laboratory for Molecular Sciences, Key Laboratory of Polymer Chemistry and Physics of Ministry of Education, Center for Soft Mater Science and Engineering, College of Chemistry and Molecular Engineering, Peking University, Beijing 100871, China*

Complete contact information is available at: https://pubs.acs.org/10.1021/acsmacrolett.1c00282

Notes

The authors declare no competing financial interest.

■ ACKNOWLEDGMENTS

The authors acknowledge financial support from the National Natural Science Foundation of China (NSFC; Grant Nos. 22073002, 21634001, and 21674005) and the Natural Science and Engineering Research Council (NSERC) of Canada.

■ REFERENCES

(1) Brangwynne, C. P.; Eckmann, C. R.; Courson, D. S.; Rybarska, A.; Hoege, C.; Gharakhani, J.; Julicher, F.; Hyman, A. A. Germline P Granules Are Liquid Droplets That Localize by Controlled Dissolution/Condensation. *Science* **2009**, *324*, 1729−1732.

(2) Crowe, C. D.; Keating, C. D. Liquid−liquid phase separation in artificial cells. *Interface Focus* **2018**, *8*, 20180032.

(3) Koga, S.; Williams, D. S.; Perriman, A. W.; Mann, S. Peptide−nucleotide microdroplets as a step towards a membrane-free protocell model. *Nat. Chem.* **2011**, *3*, 720−724.

(4) Aumiller, W. M.; Pir Cakmak, F.; Davis, B. W.; Keating, C. D. RNA-Based Coacervates as a Model for Membraneless Organelles: Formation, Properties, and Interfacial Liposome Assembly. *Langmuir* **2016**, *32*, 10042−10053.

(5) Poudyal, R. R.; Pir Cakmak, F.; Keating, C. D.; Bevilacqua, P. C. Physical Principles and Extant Biology Reveal Roles for RNA-Containing Membraneless Compartments in Origins of Life Chemistry. *Biochemistry* **2018**, *57*, 2509−2519.

(6) Srivastava, S.; Tirrell, M. V. *Advances in Chemical Physics*; John Wiley & Sons, Inc., 2016; pp 499−544.

(7) Fu, J.; Schlenoff, J. B. Driving Forces for Oppositely Charged Polyion Association in Aqueous Solutions: Enthalpic, Entropic, but Not Electrostatic. *J. Am. Chem. Soc.* **2016**, *138*, 980−990.

(8) Rathee, V. S.; Sidky, H.; Sikora, B. J.; Whitmer, J. K. Role of Associative Charging in the Entropy−Energy Balance of Polyelectrolyte Complexes. *J. Am. Chem. Soc.* **2018**, *140*, 15319−15328.

(9) Lou, J.; Friedowitz, S.; Qin, J.; Xia, Y. Tunable Coacervation of Well-Defined Homologous Polyanions and Polycations by Local Polarity. *ACS Cent. Sci.* **2019**, *5*, 549−557.

(10) McCarty, J.; Delaney, K. T.; Danielsen, S. P. O.; Fredrickson, G. H.; Shea, J.-E. Complete Phase Diagram for Liquid-Liquid Phase Separation of Intrinsically Disordered Proteins. *J. Phys. Chem. Lett.* **2019**, *10*, 1644−1652.

(11) Overbeek, J. T. G.; Voorn, M. J. Phase separation in polyelectrolyte solutions. Theory of complex coacervation. *J. Cell. Comp. Physiol.* **1957**, *49*, 7−26.

(12) Salehi, A.; Larson, R. G. A Molecular Thermodynamic Model of Complexation in Mixtures of Oppositely Charged Polyelectrolytes with Explicit Account of Charge Association/Dissociation. *Macromolecules* **2016**, *49*, 9706−9719.

(13) Castelnovo, M.; Joanny, J.-F. Complexation between oppositely charged polyelectrolytes: Beyond the Random Phase Approximation. *Eur. Phys. J. E: Soft Matter Biol. Phys.* **2001**, *6*, 377−386.
(14) Kudlay, A.; Olvera de la Cruz, M. Precipitation of oppositely charged polyelectrolytes in salt solutions. *J. Chem. Phys.* **2004**, *120*, 404−412.
(15) Kudlay, A.; Ermoshkin, A. V.; Olvera de la Cruz, M. Complexation of Oppositely Charged Polyelectrolytes: Effect of Ion Pair Formation. *Macromolecules* **2004**, *37*, 9231−9241.
(16) Lin, Y.-H.; Forman-Kay, J. D.; Chan, H. S. Sequence-Specific Polyampholyte Phase Separation in Membraneless Organelles. *Phys. Rev. Lett.* **2016**, *117*, 178101.
(17) Qin, J.; de Pablo, J. J. Criticality and Connectivity in Macromolecular Charge Complexation. *Macromolecules* **2016**, *49*, 8789−8800.
(18) Perry, S. L.; Sing, C. E. PRISM-Based Theory of Complex Coacervation: Excluded Volume versus Chain Correlation. *Macromolecules* **2015**, *48*, 5040−5053.
(19) Zhang, P.; Alsaifi, N. M.; Wu, J.; Wang, Z.-G. Polyelectrolyte complex coacervation: Effects of concentration asymmetry. *J. Chem. Phys.* **2018**, *149*, 163303.
(20) Lytle, T. K.; Sing, C. E. Transfer matrix theory of polymer complex coacervation. *Soft Matter* **2017**, *13*, 7001−7012.
(21) Rubinstein, M.; Liao, Q.; Panyukov, S. Structure of Liquid Coacervates Formed by Oppositely Charged Polyelectrolytes. *Macromolecules* **2018**, *51*, 9572−9588.
(22) Lee, J.; Popov, Y. O.; Fredrickson, G. H. Complex coacervation: A field theoretic simulation study of polyelectrolyte complexation. *J. Chem. Phys.* **2008**, *128*, 224908.
(23) Shen, K.; Wang, Z.-G. Polyelectrolyte Chain Structure and Solution Phase Behavior. *Macromolecules* **2018**, *51*, 1706−1717.
(24) Sing, C. E. Development of the modern theory of polymeric complex coacervation. *Adv. Colloid Interface Sci.* **2017**, *239*, 2−16.
(25) Feric, M.; Vaidya, N.; Harmon, T. S.; Mitrea, D. M.; Zhu, L.; Richardson, T. M.; Kriwacki, R. W.; Pappu, R. V.; Brangwynne, C. P. Coexisting Liquid Phases Underlie Nucleolar Subcompartments. *Cell* **2016**, *165*, 1686−1697.
(26) Lafontaine, D. L. J.; Riback, J. A.; Bascetin, R.; Brangwynne, C. P. The nucleolus as a multiphase liquid condensate. *Nat. Rev. Mol. Cell Biol.* **2021**, *22*, 165−182.
(27) Boeynaems, S.; Holehouse, A. S.; Weinhardt, V.; Kovacs, D.; Van Lindt, J.; Larabell, C.; Van Den Bosch, L.; Das, R.; Tompa, P. S.; Pappu, R. V.; Gitler, A. D. Spontaneous driving forces give rise to protein-RNA condensates with coexisting phases and complex material properties. *Proc. Natl. Acad. Sci. U. S. A.* **2019**, *116*, 7889−7898.
(28) Mountain, G. A.; Keating, C. D. Formation of Multiphase Complex Coacervates and Partitioning of Biomolecules within them. *Biomacromolecules* **2020**, *21*, 630−640.
(29) Lu, T.; Spruijt, E. Multiphase Complex Coacervate Droplets. *J. Am. Chem. Soc.* **2020**, *142*, 2905−2914.
(30) Moreau, N. G.; Martin, N.; Gobbo, P.; Tang, T.-Y. D.; Mann, S. Spontaneous membrane-less multi-compartmentalization via aqueous two-phase separation in complex coacervate micro-droplets. *Chem. Commun.* **2020**, *56*, 12717−12720.
(31) Holehouse, A. S.; Pappu, R. V. Functional Implications of Intracellular Phase Transitions. *Biochemistry* **2018**, *57*, 2415−2423.
(32) Sear, R. P.; Cuesta, J. A. Instabilities in Complex Mixtures with a Large Number of Components. *Phys. Rev. Lett.* **2003**, *91*, 245071.
(33) Jacobs, W. M.; Frenkel, D. Predicting phase behavior in multicomponent mixtures. *J. Chem. Phys.* **2013**, *139*, 024108.
(34) Jacobs, W. M.; Frenkel, D. Phase Transitions in Biological Systems with Many Components. *Biophys. J.* **2017**, *112*, 683−691.
(35) Mao, S.; Kuldinow, D.; Haataja, M. P.; Košmrlj, A. Phase behavior and morphology of multicomponent liquid mixtures. *Soft Matter* **2019**, *15*, 1297−1311.
(36) Chen, Y.; Yuan, M.; Zhang, Y.; Liu, S.; Yang, X.; Wang, K.; Liu, J. Construction of coacervate-in-coacervate multi-compartment protocells for spatial organization of enzymatic reactions. *Chem. Sci.* **2020**, *11*, 8617−8625.
(37) Danielsen, S. P. O.; McCarty, J.; Shea, J.-E.; Delaney, K. T.; Fredrickson, G. H. Molecular design of self-coacervation phenomena in block polyampholytes. *Proc. Natl. Acad. Sci. U. S. A.* **2019**, *116*, 8224−8232.
(38) Shen, K.; Wang, Z.-G. Electrostatic correlations and the polyelectrolyte self energy. *J. Chem. Phys.* **2017**, *146*, 084901.
(39) Spruijt, E.; Westphal, A. H.; Borst, J. W.; Cohen Stuart, M. A.; van der Gucht, J. Binodal Compositions of Polyelectrolyte Complexes. *Macromolecules* **2010**, *43*, 6476−6484.
(40) Wolff, J.; Marques, C. M.; Thalmann, F. Thermodynamic Approach to Phase Coexistence in Ternary Phospholipid-Cholesterol Mixtures. *Phys. Rev. Lett.* **2011**, *106*, 128104.
(41) Borue, V. Y.; Erukhimovich, I. Y. A statistical theory of globular polyelectrolyte complexes. *Macromolecules* **1990**, *23*, 3625−3632.
(42) Jing, H.; Bai, Q.; Lin, Y.; Chang, H.; Yin, D.; Liang, D. Fission and Internal Fusion of Protocell with Membraneless "Organelles" Formed by Liquid−Liquid Phase Separation. *Langmuir* **2020**, *36*, 8017−8026.
(43) Adhikari, S.; Prabhu, V. M.; Muthukumar, M. Lower Critical Solution Temperature Behavior in Polyelectrolyte Complex Coacervates. *Macromolecules* **2019**, *52*, 6998−7004.
(44) Adhikari, S.; Leaf, M. A.; Muthukumar, M. Polyelectrolyte complex coacervation by electrostatic dipolar interactions. *J. Chem. Phys.* **2018**, *149*, 163308.
(45) Lytle, T. K.; Chang, L.-W.; Markiewicz, N.; Perry, S. L.; Sing, C. E. Designing Electrostatic Interactions via Polyelectrolyte Monomer Sequence. *ACS Cent. Sci.* **2019**, *5*, 709−718.
(46) Rumyantsev, A. M.; Jackson, N. E.; Yu, B.; Ting, J. M.; Chen, W.; Tirrell, M. V.; de Pablo, J. J. Controlling Complex Coacervation via Random Polyelectrolyte Sequences. *ACS Macro Lett.* **2019**, *8*, 1296−1302.
(47) Trejo-Ramos, M. A.; Tristán, F.; Menchaca, J.-L.; Pérez, E.; Chávez-Páez, M. Structure of polyelectrolyte complexes by Brownian dynamics simulation: Effects of the bond length asymmetry of the polyelectrolytes. *J. Chem. Phys.* **2007**, *126*, 014901.
(48) Shakya, A.; Girard, M.; King, J. T.; Olvera de la Cruz, M. Role of Chain Flexibility in Asymmetric Polyelectrolyte Complexation in Salt Solutions. *Macromolecules* **2020**, *53*, 1258−1269.

https://doi.org/10.1021/acsmacrolett.1c00282
ACS Macro Lett. 2021, 10, 1041−1047